Charge ordering at room temperature in $Tb_{0.5}Ca_{0.5}MnO_3$

1997 J. Phys.: Condens. Matter 9 10321

(http://iopscience.iop.org/0953-8984/9/47/002)

J. Phys.: Condens. Matter **9** (1997) 10321–10331. Printed in the UK PII: S0953-8984(97)83861-1

Charge ordering at room temperature in $Tb_{0.5}Ca_{0.5}MnO_3$

J Blasco†, J García†, J M de Teresa†, M R Ibarra†, J Pérez†, P A Algarabel†, C Marquina† and C Ritter‡

† Departamento de Física de la Materia Condensada e Instituto de Ciencia de Materiales de Aragón, Universidad de Zaragoza–Consejo Superior de Investigaciones Científicas, 50009 Zaragoza, Spain

‡ Institut Laue–Langevin, Boîte Postale 156, 38042 Grenoble Cédex, France

Received 30 April 1997, in final form 26 August 1997

Abstract. $Tb_{0.5}Ca_{0.5}MnO_3$ has been studied by means of a.c. magnetic susceptibility, x-ray and neutron diffraction from 1.5 up to 330 K. This compound shows a structural transition at 299.7 K. Below this temperature a charge ordering state was observed by both x-ray and neutron diffraction measurements. The structure is orthorhombic at temperatures higher than 300 K, but at lower temperatures the patterns show new reflection peaks that can be accounted for in a monoclinic unit cell with stripes of Mn^{3+} and Mn^{4+} in the *ac*-plane. Moreover, the system orders antiferromagnetically at around 120 K giving rise to a magnetic structure of CE type. The magnetic susceptibility measurement clearly shows an anomalous behaviour at both transition temperatures. The charge ordering temperature for the $Tb_{0.5}Ca_{0.5}MnO_3$ compound is the highest reported in the $RE_{0.5}Ca_{0.5}MnO_3$ series (RE = rare earth). This is argued to be a consequence of the larger orthorhombic distortion produced in the unit cell by the lower size of Tb^{3+} ion.

1. Introduction

Mixed oxides of Mn and rare earth (RE) have became one of the topics of major interest in recent years due to a rich variety of properties [1–5]. As an example, the $La_{1-x}Ca_xMnO_3$ series shows different magnetic structures at low temperature when varying the calcium content. The two end members of this series are both insulator and antiferromagnetic (AF). The AF ordering is due to the superexchange interaction of Mn^{3+} or Mn^{4+} and, in addition, $LaMnO_3$ shows static Jahn–Teller (JT) distortion of MnO_6 octahedra [6].

Partial substitution of La for Ca in $LaMnO_3$ gives rise to ferromagnetic ordering at low temperatures for $x \leqslant 0.5$. An insulator–metal (IM) transition is induced at the ferromagnetic ordering temperature (T_c) for $0.5 \geqslant x > 0.15$. This feature was explained in the past by the so-called double exchange interaction proposed by Zener [7]. The metallic behaviour can be induced by an applied external magnetic field which gives rise to the appearance of giant magnetoresistance (GMR). The maximum value of GMR is reached at $x = 0.33$ [4]. Strong electron–phonon coupling has been observed above T_c for these compounds [3] and magnetic polaron formation above ferromagnetic ordering has been suggested to be the driving force for GMR [8]. Moreover, evidence for JT effects have been detected in samples with higher Ca contents where charge ordering (CO) is developed. CO takes place in 3d narrow-band systems when the long-range Coulomb interaction among the carriers is predominant over the kinetic energy of the charge carriers [9]. CO is best observed in systems where the carrier concentration corresponds to a certain fraction of lattice points,

0953-8984/97/4710321+11$19.50

being particularly optimized at $x = 0.5$. CO prevails at low temperatures in $La_{0.5}Ca_{0.5}MnO_3$ and simultaneous AF ordering is developed at lower temperatures than T_c [10]. For $x > 0.5$, where there is no ferromagnetism, CO is formed at temperatures (T_{CO}) higher than the AF ordering [11, 12].

Goodenough pointed out in the fifties that ordered-bond arrangements, arising from different kinds of Mn ion, can result in cooperative lattice strains [13]. He proposed three possible Mn^{3+}/Mn^{4+} arrangements in a primitive cubic cell: in alternate (111), (100) or (110) planes. The optimum electrostatic configuration is obtained by ordering within (100) planes. This kind of arrangement has been suggested from electron microscopy studies for the $Pr_{1-x}Ca_xMnO_3$ and $Nd_{1-x}Ca_xMnO_3$ series [14, 15]. Recently, a structural model has been proposed by Radaelli *et al* [16] to account for CO in the $La_{0.5}Ca_{0.5}MnO_3$ compound. They have found superstructure peaks arising from doubling the a-axis of the high-temperature orthorhombic lattice. This implies an Mn^{3+}/Mn^{4+} arrangement in the (100) orthorhombic plane, i.e. an ordering within (110) primitive cubic planes. Notice the relation between the orthorhombic and the primitive cubic unit cell vectors: $\boldsymbol{a}_o = \boldsymbol{a}_c + \boldsymbol{b}_c$, $\boldsymbol{b}_o = \boldsymbol{a}_c - \boldsymbol{b}_c$; $\boldsymbol{a}_c$ and $\boldsymbol{b}_c$ being the cubic cell vectors, $\boldsymbol{a}_o$ and $\boldsymbol{b}_o$ being the orthorhombic cell vectors. The result obtained by Radaelli *et al* [16] corresponds to a monoclinic cell with the following lattice parameters: $2 \times a$, b, c and $\beta \approx 90$; a, b and c being the lattice parameters of the high-temperature orthorhombic unit cell. This new structure accounts for Mn^{3+}/Mn^{4+} ordering in stripes along the new ac-plane. In fact, a similar model was proposed in the past by Jiràk *et al* [17] for the $Pr_{0.5}Ca_{0.5}MnO_3$ compound.

In spite of the exhaustive study on CO in samples with light rare earths (La, Pr, Nd), very little is known about these effects in samples with heavier rare earths. It is well known that replacement of La by heavier and smaller rare earths induces larger lattice distortions, thus weakening the ferromagnetic double exchange interaction [18]. This fact explains that CO is observed over a wider concentration range for the $(Pr, Nd)_{1-x}Ca_xMnO_3$ series than for $La_{1-x}Ca_xMnO_3$ samples [11, 12, 14, 15].

Here we present the study of the structural changes induced by temperature in $Tb_{0.5}Ca_{0.5}MnO_3$ by means of both x-ray and neutron diffraction. We find a structural phase transition at around room temperature that can be described by a stripe ordering of Mn ions along (110) primitive cubic planes. The CO transition has been also detected by differential scanning calorimetry (DSC). Moreover, antiferromagnetic ordering of the localized Mn^{3+} and Mn^{4+} spins was observed at low temperatures. Magnetic susceptibility nicely shows different anomalies whose temperatures coincide with the changes observed by x-ray and neutron diffraction measurements.

2. Experimental section

The sample was prepared by ceramic procedures from stoichiometric amounts of Tb_4O_7, $CaCO_3$ and $MnCO_3$. The precursors were mixed and heated at 950 °C overnight and then ground, pressed and calcined at 1250 °C for 3 d with intermediate grindings. The x-ray diffraction pattern showed that the sample was of single phase. The Mn^{4+} content was determined by redox titration using titrated potassium permanganate solution and Mohr's salt. The result was 49% Mn^{4+} that agrees with the expected value (50%) within the experimental error.

Step-scanned x-ray diffraction patterns were collected using a Rigaku D/max-B instrument with a copper rotating anode and a graphite monochromator to select the Cu Kα wavelength. The device was working at 45 kV and 160 mA and a room-temperature pattern was collected from 18° up to 140° in steps of 0.02° with a counting rate of 8 s/step. A

continuous-helium-flow cryostat from Oxford Instruments was coupled to the goniometer in order to measure at selected temperatures: 100 K, 150 K, 200 K, 250 K, 300 K, 315 K and 330 K. These patterns were collected from 5° up to 80° in steps of 0.03° and a counting rate of 3 s/step. Partial patterns were collected sometimes at low temperatures with larger counting rates (around 40 s/step) in order to notice better the superstructure peaks.

Neutron diffraction experiments were carried out at different temperatures at the high-flux reactor of the ILL using the D1B instrument working with a wavelength $\lambda = 2.52$ Å and covering an angular range $2^\circ \leqslant 2\theta \leqslant 100^\circ$. Structural refinements were made in both x-ray and neutron diffractograms by using the FULLPROF program [19].

Measurements of a.c. susceptibility were performed using a commercial Quantum Design (SQUID) magnetometer between 5 and 400 K. DSC measurements were carried out between 260 and 350 K with a scan rate of 10 K min^{-1} by using a TA-2000 instrument.

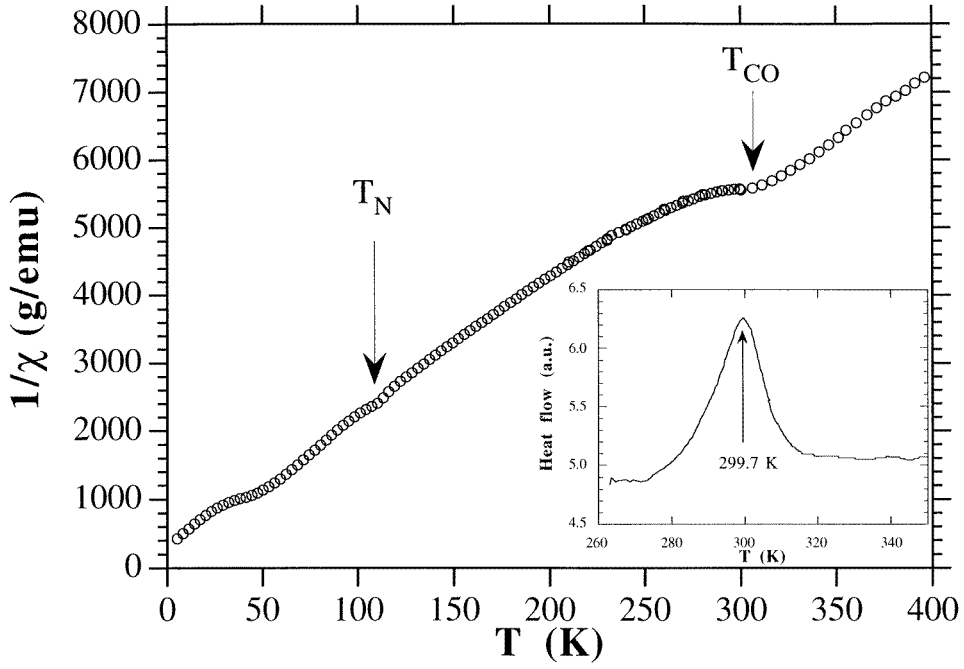

Figure 1. Inverse of the a.c. magnetic susceptibility against temperature for the $Tb_{0.5}Ca_{0.5}MnO_3$ sample. T_{CO} indicates the charge ordering temperature; T_N marks the temperature for the antiferromagnetic ordering. The inset shows DSC measurements between 260 and 350 K.

3. Results and discussion

The $1/\chi_{ac}$–T curve for the $Tb_{0.5}Ca_{0.5}MnO_3$ sample is displayed in figure 1 between 5 K and 400 K. This curve shows three anomalies at 300 K, 120 K and 50 K. The first one is associated with the developing of the charge ordering state as will be seen below when discussing the x-ray and neutron diffraction measurements. The small kink at around 120 K corresponds to the AF ordering temperature (T_N) as can be inferred from neutron experiments. Finally, the anomaly around 50 K may be ascribed to the formation of cluster-glass regions in the sample. Cluster-glasses were observed in related materials such as

$Tb_{0.66}Ca_{0.33}MnO_3$ where a cusplike anomaly [18], associated with a spin-glass behaviour, is observed in the χ_{ac} curve at 50 K. The χ_{ac} of this sample does not follow a Curie–Weiss law due to the these anomalies; nevertheless one can obtain accurate fits in two temperature ranges: between 325 and 400 K, i.e. above T_{CO}, and between 130 and 230 K, i.e. below T_{CO}. The results of both fits are summarized in table 1. Both fits give similar Curie constants as can be inferred from the similar slopes above and below T_{CO} (see figure 1). The effective magnetic moments in both cases are slightly higher than the expected for this system. The main difference between both fits concerns the Weiss constants, positive above T_{CO} and negative below T_{CO}. This feature could be an indication of the overall character of the magnetic interactions which change from ferromagnetic to AF when the charge is localized. Similar conclusions were proposed by Wei Bao *et al* [20] in the study of the (Bi, Ca)MnO_3 system. The CO transition can be also detected by means of DSC measurements. The inset of figure 1 displays the large endothermic peak at $T_{CO} = 299.7$ K in the heat capacity curve.

Table 1. Magnetic constants and effective magnetic moment (Bohr magnetons per formula unit) from the a.c. magnetic susceptibility of $Tb_{0.5}Ca_{0.5}MnO_3$ fitted to a Curie–Weiss law: $\chi = C/(T - \theta)$.

	130 K–230 K	325 K–400 K
C (emu K g^{-1})	0.052	0.050
θ (K)	24	−34
μ_{eff} (μ_B f.u.$^{-1}$)	9.15	9.0

X-ray diffractograms between 100 and 330 K show the same main diffraction peaks which can be indexed on the basis of an orthorhombic unit cell with *Pnma* space group, very common in this family of oxides. Nevertheless, several differences can be observed. First, all patterns collected below 300 K show very weak new reflections as shown in figure 2 where the diffractograms at 100 and 330 K are compared. The insets show in detail the appearance of these new peaks. Secondly, diffraction patterns at around room temperature show a broadening of diffraction peaks in agreement with previous results in related systems [10, 21]. Such broadening can arise from the diffuse scattering due to small domains of Mn^{3+}/Mn^{4+} ordering with some degree of coherence. The growth of these domains at temperatures lower than T_{CO} gives rise to the new satellite peaks. In table 2, we summarize the results obtained from a profile analysis at selected temperatures. In this analysis an orthorhombic unit cell and an average Debye–Waller factor were used. When individual Debye–Waller factors are used for each atom, large values of these factors are obtained at low temperatures, specially for oxygen atoms. This is an indication of disorder or distortions not considered in an orthorhombic model. The pattern obtained at the highest temperature (330 K) gives the best reliability factors for the fit. Fitting the patterns at 300 or 315 K results in poorer reliability factors due to the above-mentioned broadening of the diffraction peaks, while at lower temperatures the new reflections cannot be accounted for in an orthorhombic cell. These new reflections can be indexed by doubling the a-axis of the high-temperature orthorhombic lattice as indicated in figure 2(b). Nevertheless, the peak positions do not coincide exactly by doubling the a-parameter indicating an incommensurate lattice in agreement with previous results obtained by Radaelli *et al* for $La_{0.5}Ca_{0.5}MnO_3$ [16]. The similar features for both compounds suggest the existence of a common superstructure at low temperatures for the $RE_{0.5}Ca_{0.5}MnO_3$ series, which arises from an ordering of Mn^{3+} and Mn^{4+} within (110) planes of the primitive cubic cell. This superstructure has been reported

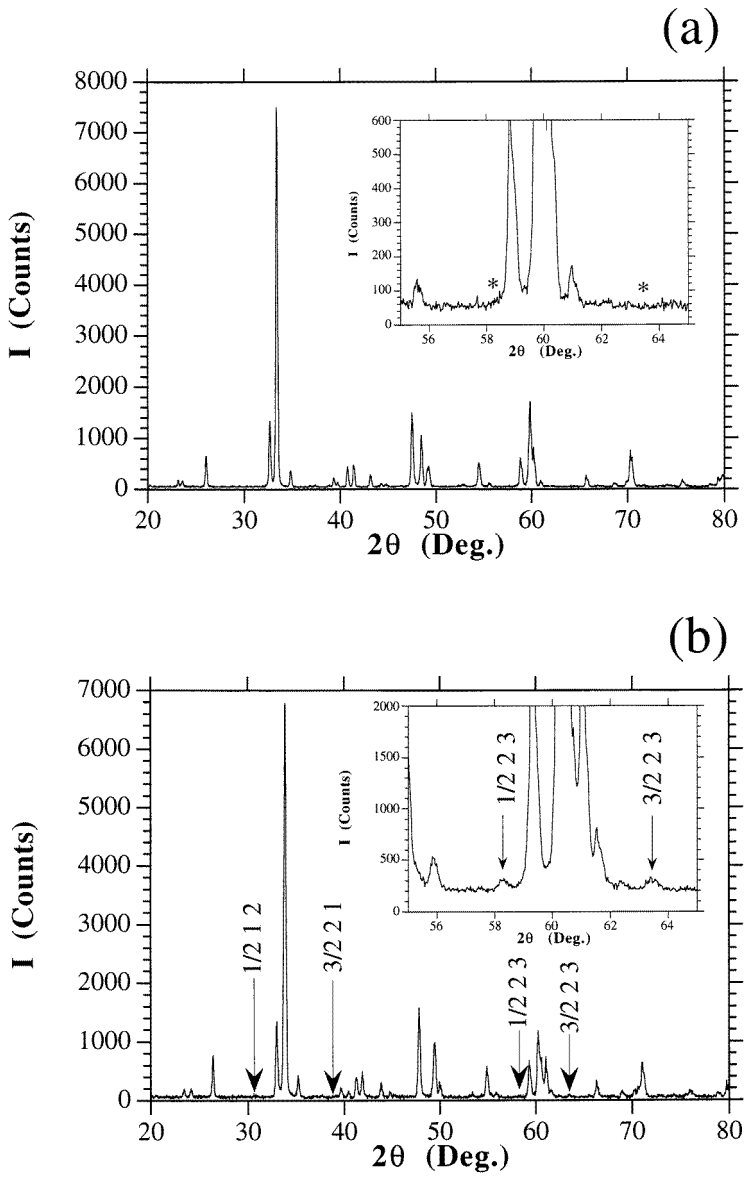

Figure 2. (a) X-ray diffraction pattern at 330 K of the $Tb_{0.5}Ca_{0.5}MnO_3$ sample (the inset shows the absence of superstructure peaks whose calculated positions are indicated by asterisks in the pattern); (b) x-ray diffraction pattern at 100 K of the $Tb_{0.5}Ca_{0.5}MnO_3$ sample (the arrows indicate the position and indexes of the detected superstructure peaks). The inset shows a detail of some superstructure peaks of the pattern at 100 K.

recently for $La_{0.5}Ca_{0.5}MnO_3$ and can be derived from the high-temperature orthorhombic cell, *Pnma*, by doubling the *a*-axis. This results in a monoclinic cell with a space group $P2_1/m$. In this space group there are four sites for Tb or Ca (hereafter denoted by RE), three for Mn and eight for O with a total of 31 positional parameters. Due to the weakness of extra reflections and the large amount of positional parameters, an accurate fit of the x-ray pattern

Table 2. Refined fractional atomic positions, average Debye–Waller factor, unit-cell parameters, reliability factors (%) and interatomic distances between Mn and O atoms (Å) for $Tb_{0.5}Ca_{0.5}MnO_3$ at selected temperatures ($Z = 4$). All patterns were refined in the *Pnma* space group (No 62). Mn is located at (4b): $(00\frac{1}{2})$. Numbers in parentheses are statistical errors of the last significant digits.

	100 K	300 K	315 K	330 K
Tb/Ca	−0.0501(4)	−0.0512(3)	−0.0511(3)	−0.0508(2)
	$\frac{1}{4}$	$\frac{1}{4}$	$\frac{1}{4}$	$\frac{1}{4}$
	0.0092(7)	0.0104(6)	0.0102(5)	0.0102(3)
O(1)	0.5291(29)	0.5297(24)	0.5284(22)	0.5240(15)
	$\frac{1}{4}$	$\frac{1}{4}$	$\frac{1}{4}$	$\frac{1}{4}$
	−0.0968(32)	−0.1004(30)	−0.0927(29)	−0.0913(19)
O(2)	0.2109(25)	0.2093(20)	0.2093(19)	0.2088(13)
	0.4519(15)	0.4591(14)	0.4588(14)	0.4578(9)
	0.2147(30)	0.2088(24)	0.2097(23)	0.2059(15)
B (Å^2)	1.64(10)	0.99(7)	0.94(7)	1.01(3)
a (Å)	5.4526(4)	5.4618(3)	5.4571(3)	5.4561(1)
b (Å)	7.3961(6)	7.4717(4)	7.4783(4)	7.4854(2)
c (Å)	5.3358(4)	5.3370(3)	5.3325(3)	5.3316(1)
R_{wp}	19.2	15.9	15.7	11.6
R_B	7.1	5.5	5.9	5.4
Mn–O(1)	1.926(5)	1.950(4)	1.940(4)	1.938(3)
Mn–O(2)	1.981(14)	1.964(12)	1.965(11)	1.964(7)
	1.941(15)	1.953(12)	1.948(12)	1.957(7)

seems to be meaningless. The presence of superstructure peaks in the x-ray diffraction pattern confirms, however, the atomic origin of the new peaks. The origin of this transition can be visualized as follows: the electronic delocalization at high temperature makes all Mn ions equivalent from a crystallographic point of view. The electronic localization at low temperature produces local strain around the Mn atoms due to the different ionic size of Mn^{3+} and Mn^{4+} on the one hand, and the JT effect of a Mn^{3+} on the other. The long-range cooperative strain can result in a new superstructure. In fact, the diffraction techniques can detect the cooperative strain associated with different kind of Mn ion in the cell instead of the proper Mn^{3+}/Mn^{4+} order. At lower temperatures, magnetic interaction between Mn ions gives rise to long-range magnetic ordering as is observed in neutron diffraction experiments.

The thermal scan of neutron diffractograms for $Tb_{0.5}Ca_{0.5}MnO_3$ is plotted in figure 3. Extra AF peaks develop at about 140 K. The magnetic structure at low temperatures is of CE type, similar to that reported for $Pr_{0.5}Ca_{0.5}MnO_3$ [17]. The CE-type structure was described in the fifties and can be viewed as a coherent stacking of unit cells with C- and E-type structures. In the C-type cell all Mn atoms have two ferro- and four antiferromagnetic nearest neighbours whereas the reverse is true for the E-type cell. All of these magnetic structures have been described in detail by Wollan and Koehler [22]. The reflections associated with a charge ordering were first detected in these neutron diffraction patterns but their intensities are so low that it is hard to notice them in figure 3. They begin to appear in the pattern at 300 K but changes in the lattice parameters are already visible at 310 K, the upper limit of our experimental setup. Figure 4 shows the temperature dependence of the orthorhombic

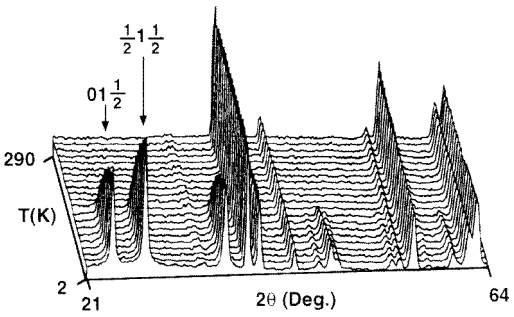

Figure 3. Neutron diffraction thermodiffractograms of the $Tb_{0.5}Ca_{0.5}MnO_3$ compound between 2 and 290 K. Arrows indicate the indexes for the first two magnetic peaks that appear at 140 K. The Miller indexes are referred to the high-temperature unit cell. The magnetic structure is obtained by doubling the *a*- and *c*-axes of the high-temperature nuclear structure.

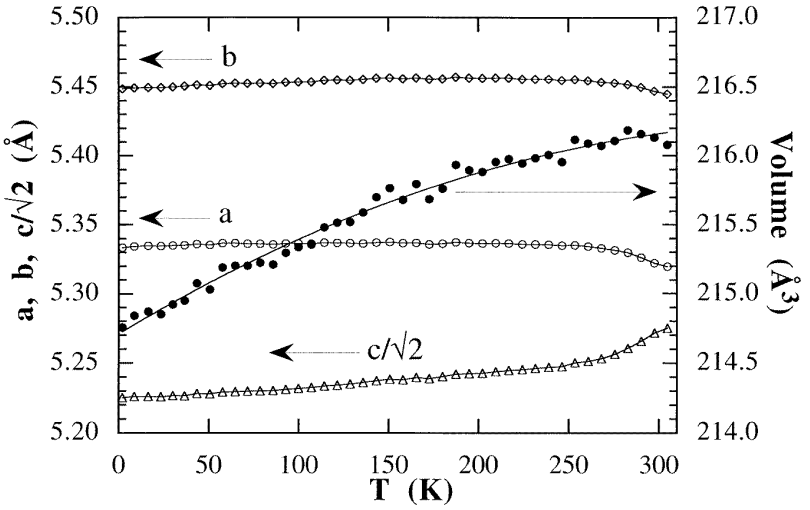

Figure 4. Thermal dependence of the orthorhombic lattice parameters and unit-cell volume of $Tb_{0.5}Ca_{0.5}MnO_3$ obtained from the Rietveld refinement of the neutron diffraction spectra.

lattice parameters obtained from a profile refinement of the neutron diffraction data. Both *a*- and *b*-axes show a slight increase at T_{CO} while the *c*-axis decreases. Nevertheless, no changes were observed at T_N. These features are similar to those reported for other related systems with CO and AF ordering [10, 12]. In order to account for the structural changes induced by the CO, the neutron diffractogram obtained at 1.5 K was fitted to the above-mentioned monoclinic structure ($P2_1/m$) using several constrains. We have started from atomic positions obtained from the refinement of the structure in the *Pnma* space group by doubling the *a*-axis as displayed in figure 5. In a first step, the *z*-coordinate of Mn3 was left free (see table 3 and figure 5). Secondly, the *z*-parameters of RE1 and RE2 were allowed to follow the shift of Mn3. Finally, the *z*-parameters for oxygen atoms of the Mn3-O_6 octahedra were refined. These parameters were coupled as follow: the apical oxygens, i.e. O2 and O4, were moved in opposite directions while equatorial oxygens, i.e.

O5–O8, were moved all together in the same direction. This model gives rise only to four more free parameters compared to the *Pnma* structure and the reliability factors improve significantly. Figure 6 shows the fit of the neutron diffractogram at 1.5 K considering the $P2_1/m$ monoclinic unit cell and the results of the refinement are summarized in table 3. Moreover, the interatomic distances for Mn and O atoms are collected in table 4. It is possible to infer the existence of two kinds of Mn ion from the calculated Mn–O distances. The first set of Mn ions, Mn1 and Mn2, have two Mn–O distances larger than the other four as can be expected for a JT ion so they can be ascribed to Mn^{3+}. A second set of Mn ions, Mn3, have similar Mn–O distances. However, the values found for Mn–O distances are slightly higher than the average in Mn^{4+} oxides. This fact could arise from the simplicity of the model used. Further refinement of atomic parameters could be performed considering a $P2_1/m$ monoclinic cell. As an example, the x- and y-parameters for Mn3 and of the equatorial oxygens are free to vary in $P2_1/m$. Finally, one could expect a monoclinic cell with an arrangement of distorted Mn^{3+}–O_6 octahedra, due to the JT effect, and undistorted Mn^{4+}–O_6 octahedra in rows along the *ac*-plane as has been postulated for related compounds [16, 17, 21]. However, the large number of free parameters suggests that diffraction studies on single crystals would be needed to reach a definite conclusion.

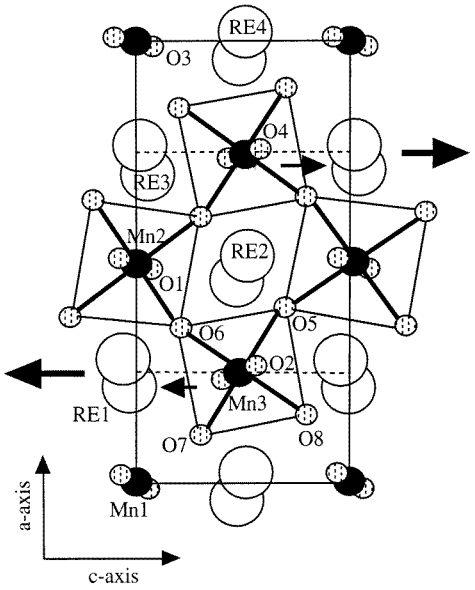

Figure 5. Projection onto the (001) plane of the $Tb_{0.5}Ca_{0.5}MnO_3$ structure at low temperatures. The atoms are denoted as follow: black circles for Mn, white circles for Tb/Ca atoms (denoted by RE) and circles with dots for O. The atoms are labelled as indicated in table 3. Full lines show the monoclinic unit cell and the MnO_6 octahedra while the dashed line indicates the high-temperature orthorhombic unit cell. Atomic shifts for RE atoms and the MnO_6 octahedron produced at the CO transition are indicated by arrows.

The high value obtained for T_{CO} can be correlated with the RE^{3+} ion size because it determines the Mn–O–Mn bond angle that governs the charge transfer integral in these oxides [2, 4]. It is well known that substitution of La for heavier rare earths such as Tb produces an increase in the orthorhombic distortion of the unit cell and, consequently, a decrease of Mn–O–Mn bond angle [18]. This fact leads to a narrowing

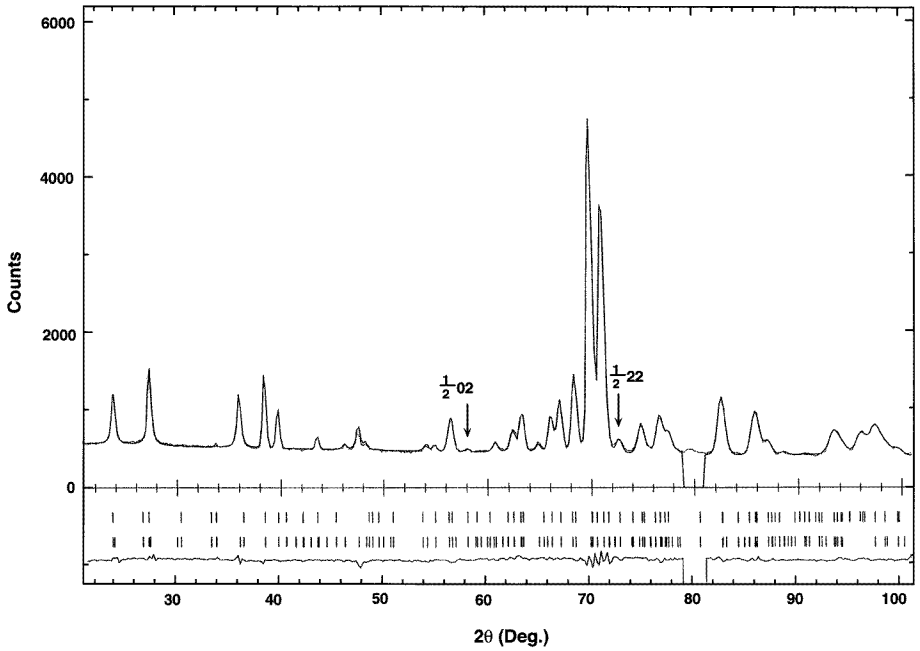

Figure 6. Rietveld refinement plot of the neutron powder diffraction data for $Tb_{0.5}Ca_{0.5}MnO_3$ at 1.5 K. The bars indicate the allowed Bragg reflections and the difference curve between observed and calculated profiles is plotted at the bottom. Arrows indicate the detected superstructure peaks due to the CO transition whose Miller indexes are referred to the high-temperature phase.

of the one-electron e_g band-width and, therefore, electronic localization is favoured. In addition, the large distortion produced by Tb atoms disfavours the electron hopping between neighbour manganeses and, consequently, it produces a weakening of the double exchange ferromagnetic interaction which accounts for the absence of ferromagnetic ordering in $Tb_{0.5}Ca_{0.5}MnO_3$. In the same way, T_N is lower for $Tb_{0.5}Ca_{0.5}MnO_3$ than for $RE_{0.5}Ca_{0.5}MnO_3$ (RE = La, Pr, Nd) because the AF superexchange interaction also depends on $\cos^2$(Mn–O–Mn) as has been established in related oxides [23].

4. Conclusions

Mn atoms in $Tb_{0.5}Ca_{0.5}MnO_3$ develop a CO structure below 300 K indicated by the presence of small superstructure peaks in both x-ray and neutron patterns. The new structure at low temperatures is monoclinic as has been reported for the $La_{0.5}Ca_{0.5}MnO_3$ compound, indicating a common structure for this series. Manganese ions develop an AF order of CE type below 140 K. Both kinds of arrangement also occur in related $RE_{0.5}Ca_{0.5}MnO_3$ perovskites but T_{CO} for $Tb_{0.5}Ca_{0.5}MnO_3$ is the highest observed while T_N is the lowest, i.e. the difference between T_{CO} and T_N for $Tb_{0.5}Ca_{0.5}MnO_3$ is the highest reported in the $RE_{0.5}Ca_{0.5}MnO_3$ perovskites. Moreover, no ferromagnetic order is developed in $Tb_{0.5}Ca_{0.5}MnO_3$ in contrast to $La_{0.5}Ca_{0.5}MnO_3$ behaviour. These features have been correlated with the rare earth ion size.

Table 3. Refined fractional atomic positions in the $P2_1/m$ space group (No 11), unit-cell parameters and reliability factors (%) for $Tb_{0.5}Ca_{0.5}MnO_3$ at 1.5 K ($Z = 8$). An average Debye–Waller factor, $B = 0.04$, was fixed for all atoms. Numbers in parentheses are statistical errors of the last significant digits.

	x	y	z
Tb/Ca(1)	0.2749	$\frac{1}{4}$	−0.0322(37)
Tb/Ca(2)	0.4751	$\frac{3}{4}$	0.4900
Tb/Ca(3)	0.7749	$\frac{1}{4}$	0.0122(37)
Tb/Ca(4)	0.9751	$\frac{3}{4}$	0.4900
Mn(1)	0	0	0
Mn(2)	$\frac{1}{2}$	0	0
Mn(3)	$\frac{1}{4}$	0	0.4809(35)
O(1)	0.4887	$\frac{1}{4}$	0.0814
O(2)	0.2613	$\frac{3}{4}$	0.5611(46)
O(3)	0.9887	$\frac{1}{4}$	0.0814
O(4)	0.7613	$\frac{3}{4}$	0.6055(46)
O(5)	0.3974	0.0437	0.6827(14)
O(6)	0.3526	0.9563	0.1827(14)
O(7)	0.1026	0.9563	0.2726(14)
O(8)	0.1474	0.0437	0.7726(14)
a (Å)		10.9070(15)	
b (Å)		7.3972(11)	
c (Å)		5.3384(7)	
R_{wp}		3.0	
R_B		3.12	

Table 4. Interatomic distances (Å) for MnO_6 octahedra of $Tb_{0.5}Ca_{0.5}MnO_3$ at 1.5 K refined in the $P2_1/m$ space group. Numbers in parentheses are distance multiplicities and statistical errors of the last significant digits.

Mn(1)–O(3)	(×2)	1.904(2)
Mn(1)–O(7)	(×2)	1.864(6)
Mn(1)–O(8)	(×2)	2.040(5)
Mn(2)–O(1)	(×2)	1.904(2)
Mn(2)–O(5)	(×2)	2.056(6)
Mn(2)–O(6)	(×2)	1.908(5)
Mn(3)–O(2)		1.902(7)
Mn(3)–O(4)		1.910(7)
Mn(3)–O(5)		1.962(11)
Mn(3)–O(6)		1.972(16)
Mn(3)–O(7)		1.982(12)
Mn(3)–O(8)		1.945(16)

Acknowledgments

The authors acknowledge the financial support of DGYCIT under project Nos MAT96-0491, MAT96-826, and APC95-123.

References

[1] von Helmolt R *et al* 1993 *Phys. Rev. Lett.* **71** 2331
[2] Moritomo Y, Asamitsu A and Yokura Y 1995 *Phys. Rev.* B **51** 16 491
[3] Ibarra M R, Algarabel P A, Marquina C, Blasco J and García J 1995 *Phys. Rev. Lett.* **75** 3541
[4] Schiffer P, Ramirez A P, Bao W and Cheong S-W 1995 *Phys. Rev. Lett.* **75** 3336
[5] Mahendiran R, Tiwary S K, Raychaudhuri A K, Ramakrishnan T V, Mahesh R, Rangavittal N and Rao C N R 1996 *Phys. Rev.* B **53** 3348
[6] Elemans J B A A, van Laar B, van der Veen K R and Loopstra B O 1971 *J. Solid State Chem.* **3** 238
[7] Zener C 1951 *Phys. Rev.* **82** 403
[8] De Teresa J M, Ibarra M R, Algarabel P A, Ritter C, Marquina C, Blasco J, García J, del Moral A and Arnold Z 1997 *Nature* **386** 256
[9] Tomioka Y, Asamitsu A, Moritomo Y, Kuwahara H and Tokura Y 1995 *Phys. Rev. Lett.* **74** 5108
[10] Radaelli P G, Cox D E, Marezio M, Cheong S-W, Schiffer P E and Ramirez A P 1995 *Phys. Rev. Lett.* **75** 4488
[11] Ramirez A P, Schiffer P, Cheong S-W, Chen C H, Bao W, Palstra T T M, Gammel P L, Bishop D J and Zegarski B 1996 *Phys. Rev. Lett.* **76** 3188
[12] Ibarra M R, De Teresa J M, Blasco J, Algarabel P A, Marquina C, García J and Stankiewicz J 1997 *Phys. Rev.* B at press
[13] Goodenough J B 1955 *Phys. Rev.* **100** 564
[14] Tomioka Y, Asamitsu A, Kuwahara H, Moritomo Y and Tokura Y 1996 *Phys. Rev.* B **53** R1689
[15] Liu K, Wu X W, Ahn K H, Sulchek T, Chien C L and Xiao J Q 1996 *Phys. Rev.* B **54** 3007
[16] Radaelli P G, Cox D E, Marezio M and Cheong S-W 1997 *Phys. Rev.* B **55** 3015
[17] Jiràk Z, Krupicka S, Simsa Z, Dlouha M and Vratislav S 1985 *J. Magn. Magn. Mater.* **53** 153
[18] Blasco J, García J, De Teresa J M, Ibarra J M, Algarabel P A and Marquina C 1996 *J. Phys.: Condens. Matter* **8** 7427
[19] Rodriguez-Carvajal J 1993 *Physica* B **192** 55
[20] Bao Wei, Axe J D, Chen C H and Cheong S-W 1997 *Phys. Rev. Lett.* **78** 543
[21] Vogt T, Cheetham, Mahendiran R, Raychaudhuri, Mahesh R and Rao C N R 1996 *Phys. Rev.* B **54** 15 303
[22] Wollan E O and Koehler W C 1955 *Phys. Rev.* **100** 545
[23] Treves D, Eibschütz M and Coppens P 1965 *Phys. Lett.* **18** 216